






Reliability and Cost-Oriented Analysis, Comparison and Selection of Multi-Level MVdc Converters

Gayan Abeynayake , *Graduate Student Member, IEEE*, Gen Li , *Member, IEEE*, Tibin Joseph , *Member, IEEE*, Jun Liang , *Senior Member, IEEE*, and Wenlong Ming , *Member, IEEE*

Abstract—DC technology has gained considerable interest in the medium voltage applications due to the benefits over the AC counterpart. However, to utilize the full capacity of this development, the selection of a suitable power electronic converter topology is a key aspect. From the pool of voltage source converters (VSC's), it is unclear which topology is suitable for multi-megawatt applications at medium voltage dc (MVdc) levels. To address this, the paper proposes a selection guideline based on reliability and optimum redundancy levels of VSCs for MVdc applications. This will be combined with other functional factors such as operational efficiency and return-on-investment. Three candidate multi-level topologies namely three-level neutral point clamped converter (3L-NPC), modular multi-level converter (MMC) and cascaded 3L-NPC (which is being used for the first MVdc link in the U.K.) have been evaluated over two-level-VSC from ± 10 kV to ± 50 kV. Results show that with the increase of MVdc voltage level MMC shows better performance whereas at low MVdc voltage levels 3L-NPC is the prominent topology.

Index Terms—Availability, MVdc, operational efficiency, reliability, return on investment.

I. INTRODUCTION

MEDIUM voltage dc (MVdc) technology is becoming an attractive solution for distribution networks thanks to its high power transfer capability, excellent controllability and operational flexibility [1]. With the increased penetration of distributed generation and electric vehicles, active control of the state-of-the-art ac distribution system has become challenging than before. Thus, MVdc network can act as an additional layer between ac transmission and distribution networks to enhance the overall system efficiency and transfer capability.

Potential applications of voltage source converter (VSC) based MVdc range from the integration of renewable energy

sources [2], [3], traction and shipboard power systems [4], [5], smart distribution systems [6] and future offshore dc collection grids [7], [8]. In particular, the use of VSC technologies at MVdc voltage level is beneficial in terms of their applicability in weak rural and complex urban distribution networks.

Among the VSC technologies, for low voltage (LV) applications, the two-level (2 L) VSC has been considered as one of the simplest and cost-effective solutions [9]. Another candidate topology is the three-level neutral point clamped converter (3L-NPC), which offers higher efficiency and better harmonic performance compared to the 2L-VSC [10]–[12]. Due to lower switching frequencies required to maintain the harmonic levels defined in standards such as IEEE 519 [13], 3L-NPC is relatively more efficient than 2L-VSC. However, for high-voltage dc (HVdc) applications, the modular multi-level converter (MMC) has been the most favored choice due to its exceptional waveform quality, compact and modular design [14], [15].

To this end, the assessment of VSC topologies at different dc voltage levels has been a key research area that received interest recently [9], [16], [17]. This is also evidenced in the several demonstration projects that have been or being implemented around the globe. The first AC to DC conversion MVdc link demonstration project in the U.K., the “ANGLE-DC” project, aims to demonstrate the application of MVdc by converting an existing 33 kV ac double-circuit to a rigid bipolar dc circuit at ± 27 kV [18]. Due to the technological maturity of the 3L-NPC and lower cost compared to MMC, a special designed cascaded 3L-NPC (C3L-NPC) has been deployed in the “ANGLE-DC” project. However, the first multi-terminal MVdc project in China used MMCs to demonstrate and supply reliable and quality power to the distribution networks [19]. The voltage of this multi-terminal MVdc project is ± 10 kV. Other MVdc demonstration projects include the underground MVdc grid within the campus infrastructure in Aachen, Germany [20] and the MVdc system in an industrial area of Shenzhen, China [21].

Although the above projects demonstrate different MVdc technologies, the selection of VSCs for these applications were largely project dependent and varies case by case. A general MVdc converter design and optimal selection principle considering reliability, efficiency and economics are not yet considered in the open literature.

Few researches were focused on the selection of VSC on MV applications with dc solutions. In [22], the feasibility of utilizing MMC and 3L-NPC for battery energy storage applications at 10 kV dc has been evaluated based on efficiency and

Manuscript received June 22, 2020; revised November 25, 2020; accepted January 5, 2021. Date of publication January 13, 2021; date of current version November 22, 2021. This work was supported in part by the European Commission's Horizon 2020 Research & Innovation Programme (Marie Skłodowska-Curie Actions) through the project “Innovative Tools for Offshore Wind and DC Grids (InnoDC)”, under Grant 765585 and in part by the EPSRC “Sustainable urban power supply through intelligent control and enhanced restoration of AC/DC networks”, under Grant EP/T021985/1. Paper no. TPWRD-00933-2020. (Corresponding author: Gen Li.)

The authors are with the School of Engineering, Cardiff University, Cardiff CF24 3AA, U.K. (e-mail: AbeynayakePA@cardiff.ac.uk; LiG9@cardiff.ac.uk; JosephT@cardiff.ac.uk; Liangj1@Cardiff.ac.uk; MingW@cardiff.ac.uk).

Color versions of one or more figures in this article are available at <https://doi.org/10.1109/TPWRD.2021.3051531>.

Digital Object Identifier 10.1109/TPWRD.2021.3051531

capital investment. However, the long term investment benefits or redundant designs have not been investigated. Redundant designs are required for the secure and economic operation of converters [23]. At LV levels, topology reliability is not much of a concern due to lower repair times and financial loss is comparatively minimal. Thus, the $n+1$ redundant design approach is used [9]. However, at HVdc levels, the unavailability of converters may cause high revenue losses and redundancy is an important aspect. The benefits of using active redundant sub-modules (SMs) for improving the reliability of MMCs have been discussed in [24], [25]. However, the optimal redundancy level has not been considered in any of these studies.

In the converter topology assessment, redundancy level needs to be considered due to higher repair times and capital investment. Thus, the identification of the optimal redundancy level is important. To bridge this research gap and identify the suitable VSC topology for MVdc voltage levels, this paper proposes a selection criterion based on the optimal redundancy level with the consideration of the VSC reliability, preventive maintenance interval, operational efficiency, the total cost of ownership (TCO) and return on investment (ROI). The primary motivation of this paper is to investigate the feasibility of utilizing suitable multi-level VSC topologies at different MVdc voltage levels. Following the proposed selection criterion, the voltage crossover points which the candidate VSCs are suitable to have been identified for the MVdc spectrum from ± 10 kV to ± 50 kV. Finally, the practicality of the proposed selection methodology is applied to the ANGLE-DC case and tested.

II. MVDC VSCS AND RELIABILITY REQUIREMENTS

A. MVdc Converter Topologies

1) *MVdc Converter Topologies*: For 2L-VSC and 3L-NPC at MVdc voltage levels, the pole-to-pole voltage cannot be withstood by a single IGBT. Thus, series-connected IGBTs are required. Press-pack IGBTs are used for series connection of IGBTs with active redundancy where all the IGBTs are sharing the load [26]. In this paper, active redundancy is chosen considering industry practice and concerns over the passive scheme. In this paper, the series-connected IGBT group in the arms of 2L-VSC and 3L-NPC is defined as switch position (SP), as shown in Fig. 1. Considering the 2L-VSC and 3L-NPC shown in Figs. 1(a) and (b), the minimum number (k) of the required IGBT modules per SP can be calculated as

$$k = \left\lceil \frac{V_{dc}}{\alpha \times V_{IGBT}} \right\rceil, \quad (1)$$

where V_{dc} is the converter pole-to-pole voltage, α is the number of SPs per arm with $\alpha = 1$ and $\alpha = 2$ refer to 2L-VSC and 3L-NPC, respectively. The IGBT nominal voltage V_{IGBT} is defined as

$$V_{IGBT} = \eta \times V_D, \quad (2)$$

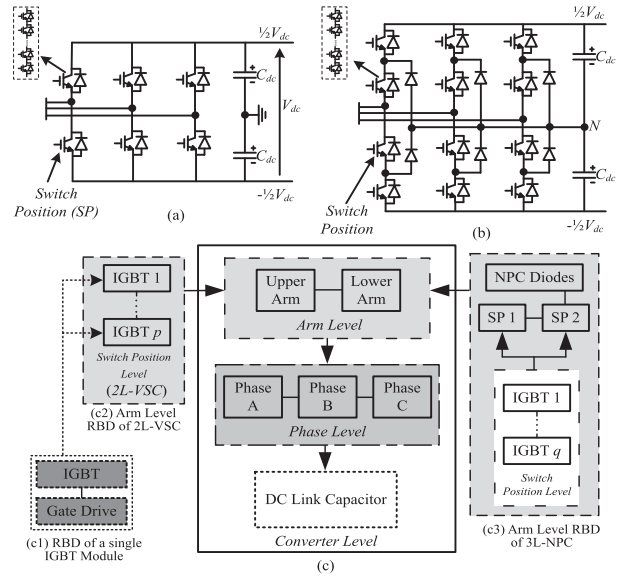


Fig. 1. Converter topologies and RBDs of 2L-VSC and 3L-NPC. (a) 2L-VSC; (b) 3L-NPC; and (c) RBDs.

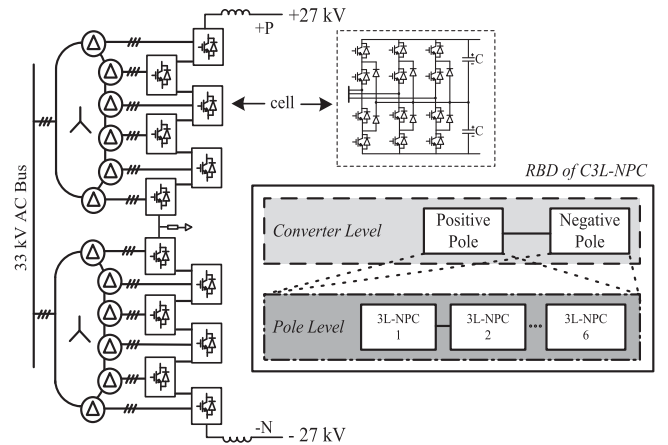


Fig. 2. Cascaded 3L-NPC topology and corresponding RBD.

where η and V_D are IGBT module de-rating factor and withstand voltage, respectively. The dc-link capacitor C_{dc} is estimated by

$$C_{dc} = \frac{2 \times S_{VSC} \times E_S}{V_{dc}^2}, \quad (3)$$

where S_{VSC} is the converter MVA rating, E_S is the energy-to-power ratio which is normally between 10-50 kJ/MVA [27].

The converter reliabilities can be obtained using the Reliability Block Diagrams (RBDs) [16]. Fig. 1(c) shows the hierarchical RBD models of the two topologies. There are different hierarchical levels in the RBDs: SP level, arm-level, phase-level and converter-level. According to the topology of the two converters, all components are required to be in a healthy state for the normal operation. Therefore, all the blocks are in series from the reliability point of view.

2) *Cascaded 3L-NPC*: Such as cascaded 2L-VSC (used in HVdc applications), 3L-NPC can also be connected in cascaded configuration as shown in Fig. 2. One of the practical examples

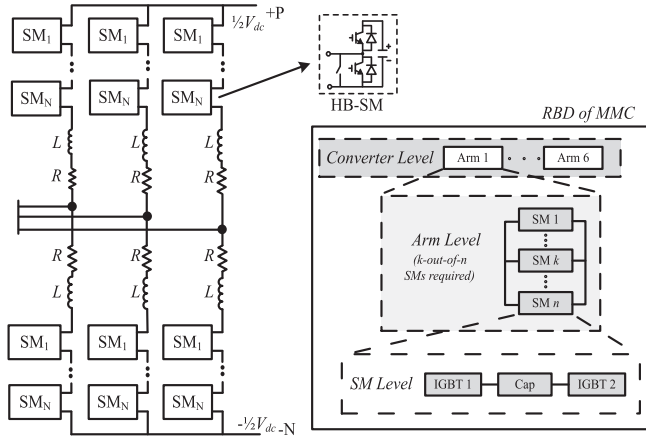


Fig. 3. MMC topology and corresponding RBD.

of such configuration is the ANGLE-DC project. It comprises of 12 cells (pole-to-pole), each of which is a 3L-NPC. Each cell is rated for 2.55 MVA with the dc-link voltage of 4.5 kV [28].

A high impedance dc grounding is applied at the converter mid-point to protect the C3L-NPC from earth faults [29]. Therefore, this is a rigid bipolar system without a monopolar operation mode. The required number of components and dc-link capacitance of each cell can be calculated using (1)–(3). The hierarchical structure of the RBD of the C3L-NPC is shown in Fig. 2.

3) *MMC*: The use of MMC at MVdc voltage level needs to be further justified in terms of reliability, efficiency and return on investment. As the capital cost and power losses of the full-bridge (FB) MMC are higher than the half-bridge (HB) MMC, the FB-MMC may not be an optimal option for MVdc applications. Therefore, only the HB-MMC is investigated in this paper, as shown in Fig. 3. As illustrated in the RBD of the HB-MMC, the redundant SMs are added at the arm level. To model the reliability of the HB-SM, the reliability blocks of the IGBTs and SM capacitor are connected in series irrespective of the physical configuration.

The minimum number of SMs (k_{SM}) required per arm can be calculated as

$$k_{SM} = \left\lceil \frac{V_{dc}}{V_{SM}} \right\rceil, \quad (4)$$

where V_{dc} is the MMC pole-to-pole voltage and V_{SM} is the SM nominal voltage. As defined in [30], the SM capacitance C_{SM} can be calculated as

$$C_{SM} = \frac{2 \times S_{MMC} \times E_{MMC}}{6 \times n \times V_{SM}^2}, \quad (5)$$

where S_{MMC} is the nominal capacity of the MMC; E_{MMC} is the nominal energy per MVA stored in the MMC; n is the number of SMs in each arm.

B. Reliability Modelling

In converter level reliability analysis, the stochastic failure nature of power electronic (PE) devices can be represented by the well-known “bathtub” curve [17], [25], [31]. In this paper,

the intrinsic failure period is assumed considering the typical project lifetime of MV distribution networks. Mathematically, the reliability function $R(t)$ of any PE device with a failure rate $\lambda(t)$ is defined as

$$R(t) = e^{-\int_0^t \lambda(t) dt}. \quad (6)$$

Assuming the useful life period is characterized by a constant value, the reliability function is calculated

$$R(t) = e^{-\lambda t}. \quad (7)$$

Unscheduled outages are associated with high costs due to the long repair time and the high amount of energy not served. These uncertain outages can be reduced with redundant designs. However, more redundant modules will increase capital investment. Therefore, an optimal redundancy level for a specific project is required. There are two main redundancy schemes which can be utilized in PE converters: the active and passive (standby) mode [32]. In the passive redundancy, redundant modules are kept idle and disconnected (or bypassed) until an operating module fails. Whereas in the active redundancy, the total dc bus voltage is shared by all the n IGBTs/modules until k minimum required modules are in operation. In this paper, active redundancy is chosen from a practical point of view.

According to the RBDs shown in Figs. 1~3, the reliability $R_a(t)$ of an SP (2L-VSC, 3L-NPC) or an arm (MMC) or pole (C3L-NPC) can be calculated with the probability theory applied for k -out-of- n systems [17].

$$R_a(t) = \sum_{i=k}^n C_n^i [R_y(t)]^i [1 - R_y(t)]^{n-i}. \quad (8)$$

In (8) $R_y(t)$ is defined as

$$R_y(t) = \begin{cases} R_{IGBT}(t) & 2L-VSC, 3L-NPC \\ R_{SM}(t) & MMC \\ R_{cell}(t) & C3L-NPC \end{cases} \quad (9)$$

where

$$R_{SM}(t) = R_{IGBT,1}(t) \times R_{IGBT,2}(t) \times R_{cap,SM}(t). \quad (10)$$

In (9), $R_{IGBT}(t)$ is the IGBT module reliability and $R_{cell}(t)$ is the reliability of the 3L-NPC which is used for the C3L-NPC. In (10), $R_{IGBT,1}(t)$ and $R_{IGBT,2}(t)$ are the reliabilities of IGBTs within the SM. $R_{cap,SM}(t)$ is the MMC SM capacitor reliability. Once $R_a(t)$ is calculated, the phase-level $R_{ph}(t)$ and converter level $R_{VSC}(t)$ reliabilities can be calculated as below.

$$R_{ph}(t) = [R_a(t)]^{2\alpha} \quad (11)$$

$$R_{VSC}(t) = [R_{ph}(t)]^3 \times [R_{cap}(t)]^\gamma \times [R_{npc-d}(t)]^\mu \quad (12)$$

where $R_{cap}(t)$ and $R_{npc-d}(t)$ are the reliabilities of dc-link capacitor and NPC diode respectively. The term α is the number of SPs. At present, no single dc capacitor or NPC diode is able to withstand the MVdc voltage levels discussed in this study. Thus, series connections of dc capacitors are required. The terms γ and μ stand for the number of series-connected dc capacitors and NPC diodes. To obtain the reliability of the MMC, (12) can be used with $\gamma = \mu = 0$ and $\alpha = 1$ since the failure rate of the

SM capacitor has already been included in (10). The reliability $R_{C3L}(t)$ of the C3L-NPC can be obtained once the cell level reliability $R_{cell}(t)$ is obtained following the same methodology discussed for the 3L-NPC.

C. Availability and Maintenance Requirements of MVdc Converters

The availability of a converter relies on the frequency of maintenance and repair time. At HVdc levels, periodic preventive maintenance is performed to keep operational costs low because planned outages attract much lower penalty payments than unplanned outages [33]. For example, the Crown Estate licenses for offshore wind farms around the U.K. require that the HVdc converter availability must be above 98% (including planned maintenance) [34]. The same maintenance approach can be used for MVdc applications.

In this paper, the analysis is mainly confined to the comparison of MVdc converter topologies. The availability of the cooling system and the power supply system are assumed to be the same. Further, compared to the failure rate of a converter topology which comprises of a large number of power electronics devices, the failure rate of the interfacing transformer is very low [35]. Hence, the converter transformer is assumed failure-free for the lifetime considered in this analysis. A stringent availability level of 99.99% is maintained for the SP (2L-VSC, 3L-NPC), arm (MMC) and pole (C3L-NPC) level so that the total converter availability can be maintained above 99.99% as of [32].

To calculate the availability of a converter SP/arm/pole A_a using the individual availability of IGBTs/SMs/cells, the k -out-of- n model is used as shown in (13), where A_b is the base availability of the arm/pole with no redundancy, N is the total number of IGBTs/SMs within an SP/arm/pole and M is the number of redundant modules.

$$A_a = \sum_{i=0}^M \frac{N!}{i!(N-i)!} A_b^i (1 - A_b)^{(N-i)} \quad (13)$$

$$A_b = e^{-\lambda_b T_M} \quad (14)$$

$$\lambda_b = -\frac{d[\ln R_a(t)]}{dt} \quad (15)$$

The parameter T_M in (14) is defined as the preventive maintenance interval (in years). In reliability theory, the base failure rate is defined as the system failure rate without redundancy. The base failure rate of converter SP/arm/pole λ_b is calculated as shown in (15) following (9) and (10) with $n = k$ in (8).

D. VSC Availability and Redundancy Analysis With Different Maintenance Intervals for ± 27 KV

The base failure rates of candidate VSCs for ± 27 kV MVdc voltage level can be calculated using (15) with the parameters given in Table I. The IGBT used for this analysis is ABB 5SNA 1300K450300 with a de-rating factor of 56% [26]. The gate drive unit SCALE-1SC0450E and dc capacitor of 2.7 kV and 1.5 mF from EPCOS-B25750H2448k004 with the failure

TABLE I
SYSTEM PARAMETERS AND BASE FAILURE RATES

| Symbols | Item | Value |
|-------------------|---------------------------------|----------------------|
| \bar{S}_{VSC} | Converter Rating | 30 MVA |
| V_{dc} | MVdc voltage level | ± 27 kV |
| V_{IGBT} | withstand voltage of IGBT | 4.5 kV |
| η | derating factor of IGBT module | 56% |
| V_{nom} | nominal voltage of IGBT module | 2.52 kV |
| E_s | Energy stored in the VSC | 20 kJ/MVA |
| λ_{IGBT} | IGBT failure rate | 0.001752 occ/yr [32] |
| λ_{cap} | dc capacitor failure rate | 0.000876 occ/yr [32] |
| λ_{GD} | failure rate of IGBT gate drive | 0.004380 occ/yr [32] |
| λ_{npc-d} | NPC diode failure rate | 0.000438 occ/yr [36] |

TABLE II
REQUIRED MIN. NUMBER OF COMPONENTS AND BASE FAILURE RATES

| Topologies | Component Count ($n = k$) | | | Base Failure Rates (occ/yr) |
|------------|-----------------------------|------------|------------|-----------------------------|
| | IGBTs | Capacitors | NPC Diodes | |
| 2L-VSC | 132 | 240 | - | 1.2299 |
| 3L-NPC | 132 | 240 | 66 | 1.2588 |
| C3L-NPC | 144 | 168 | 72 | 1.2089 |
| MMC | 264 | 264 | - | 1.8501 |

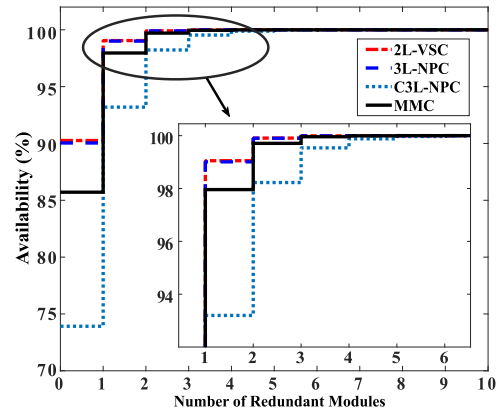


Fig. 4. Availability of ± 27 kV VSCs over redundancy for $T_M = 0.5$.

rates given in [32] are used. The selected NPC diode is ABB-5SDF13H45014 with the nominal dc voltage of 2.8 kV [36]. The calculated minimum required components and base failure rates of converters are given in Table II. Due to the higher number of components MMC shows the highest base failure rate. The C3L-NPC shows the lowest failure rate due to its lower component count. However, due to the inclusion of NPC diodes in 3L-NPC configuration, its failure rate is higher than that of 2L-VSC even though the same number of IGBTs and dc-link capacitors are used in both.

After obtaining the base failure rates of VSCs, the availability is calculated over different redundancy levels and maintenance intervals for half-year and one-year as shown in Figs. 4 and 5. The required redundant modules (which corresponds to 99.99% availability) for each topology can be obtained using the same and summarized in Table III. It can be noted that even though the base failure rate of C3L-NPC is the lowest, it requires a higher number of redundant cells to keep the same availability level ($> 99.99\%$) because its per-pole availability is the lowest amongst these VSCs due to its physical configuration.

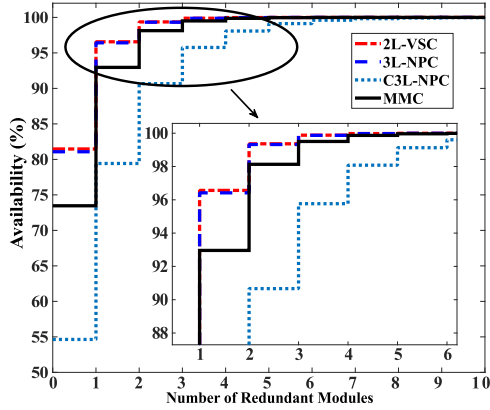
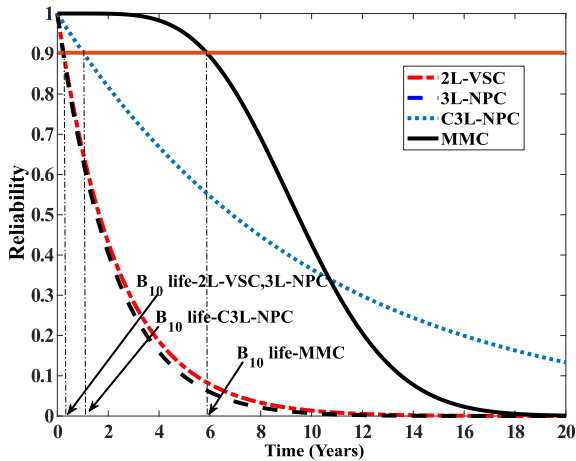

 Fig. 5. Availability of ± 27 kV VSCs over redundancy for $T_M = 1$.

 TABLE III
 REDUNDANCY LEVEL OF VSCs WITH DIFFERENT MAINTENANCE INTERVALS

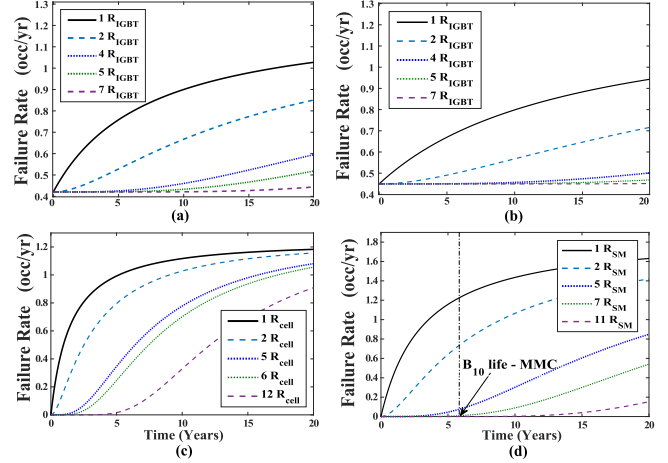
| Topologies | Minimum modules/ cells per arm | Redundant modules | |
|------------|-----------------------------------|-------------------|-----------|
| | | $T_M=0.5$ | $T_M=1$ |
| 2L-VSC | 22 | 4 (18%) | 6 (27%) |
| 3L-NPC * | 11 | 2 (18%) | 3 (27%) |
| C3L-NPC ‡ | 06 | 5 (83%) | 12 (200%) |
| MMC | 22 | 5 (22%) | 7 (31%) |

* required IGBTs per SP ‡ required cells per pole () -redundancy %


 Fig. 6. Reliability of ± 27 kV VSCs for $T_M = 0.5$ years.

Notably, with the increase of preventive maintenance interval, the redundancy level should also be increased to maintain the same availability level. Hence, the capital investment and power losses of converters may increase unnecessarily. Therefore, $T_M = 0.5$ year has been selected as the best preventive maintenance interval in the analysis.

The variation of VSC reliability for half-year maintenance interval is shown in Fig. 6. To compare VSC reliabilities on a common ground the B_{10} life can be used [25]. In reliability engineering calculations, the B_{10} life is defined as the time taken to reach 90% of the reliability of a system. It can be noted that B_{10} life of MMC is the highest with 5.9 years which is more reliable compared to other topologies. The 2L-VSC and 3L-NPC have lower B_{10} life values with 0.68 years and 0.64 years respectively. Although the MMC has the highest


 Fig. 7. Failure rates of (a) 2L-VSC; (b) 3L-NPC; (c) C3L-NPC; (d) MMC with different redundancy level for ± 27 kV with $T_M = 0.5$ years.

base failure rate, its B_{10} life is the highest after redundancy is added. The reason is, due to the cascaded structure of MMC, the capacitors are placed at SM level. When redundant SMs are added it provides additional redundancy compared to 2L-VSC and 3L-NPC which makes MMC more reliable.

Fig. 7 shows the variations of failure rate for the four topologies with different redundancy levels. It is notable that, even though the number of redundant modules is increased after the selected redundancy level, the failure rate does not increase significantly before the B_{10} life. For instance, consider the failure rates of MMC with different redundant SMs in Fig. 7(d). The failure rates correspond to B_{10} life show that below the selected optimal redundancy level (in here $R_{SM} < 5$) the MMC is more prone to fail.

III. ANALYSIS OF OPERATIONAL EFFICIENCY, TOTAL COST OF OWNERSHIP AND RETURN ON INVESTMENT

Apart from reliability and redundancy, the efficiency and lifetime cost of the VSC (i.e. TCO) are two main factors should be considered in the selection of VSCs. In [11], two types of 3L-NPC topologies are compared with the 2L-VSC for the grid integration of the type-4 wind turbine considering capital investment and operational efficiency. However, depending on the application, voltage and powers level, the associated VSC losses will change. For example, the accumulated annual energy losses of a converter utilized in MVdc distribution networks may differ from an MVdc converter applied in the offshore dc collection system.

A. Operational Efficiency

To analyze the VSCs on common ground with the general grid code requirements defined by IEEE 519 Std., the switching frequencies have been adjusted to meet the maximum current harmonic distortion limits defined in [13]. Thus, the switching frequencies of the VSCs considered for this analysis are 2.5 kHz/2L-VSC, 2 kHz/3L-NPC, 1 kHz /C3L-NPC and 100 Hz/MMC.

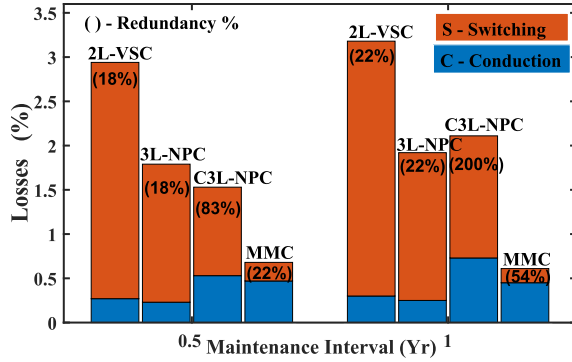


Fig. 8. VSC power losses for ± 27 kV with different maintenance intervals and redundancy.

To evaluate the switching and conduction losses of each VSC, the PLECS software tool has been used which is based on multi-dimensional lookup tables on manufacturer information at various semiconductor junction temperatures [37]. For all the losses analysis conducted, the ambient temperature was maintained at 25°C . Fig. 8 shows the percentage losses of VSCs at its rated power for ± 27 kV with different maintenance intervals for selected redundancy levels. When the maintenance interval is increased, the losses are also increased due to the utilization of more redundant modules. At $T_M = 0.5$ years, the C3L-NPC (1.52%) shows lower losses compared to 3L-NPC (1.81%) which is notable. However, due to the utilization of a greater number of redundant cells (to maintain the same availability) at $T_M = 1$ a, the losses are slightly higher than 3L-NPC. The 2L-VSC shows the highest power losses with $P_{l_{2L-0.5}} = 2.95\%$ and $P_{l_{2L-1}} = 3.17\%$. MMC presents the lowest power losses, $P_{l_{MMC-0.5}} = 0.69\%$ and $P_{l_{MMC-1}} = 0.61\%$ for both maintenance intervals.

From the perspective of mitigating converter power losses, having a lower preventive maintenance period is beneficial. Thus, for the rest of the analysis, the VSC redundancy level corresponds to $T_M = 0.5$ years has been selected.

B. Annual Energy Production

Due to variations in the demand profile of distributed loads, VSCs connected to MVdc systems may not always operate at their rated power. Thus, efficiency evaluation only at rated power may not reflect the actual efficiency of the VSC. The converter efficiencies related to different loading conditions have been obtained by varying the load current of each VSC. Obtained PLECS simulation results are shown in Fig. 9. According to Fig. 9, MMC shows the highest efficiency (above 99%) at all the loading conditions. Notably, the C3L-NPC has higher efficiency than 3L-NPC. However, at low load conditions, the converter efficiency is lower compared to the rated power due to relatively higher turn-on and turn-off losses.

To obtain a reasonable value for annual energy produced by each VSCs, a method based on the normalized load duration curve is proposed. Fig. 10 shows the normalized load duration curve for Great Britain (GB) electricity sector in 2019 [38] and

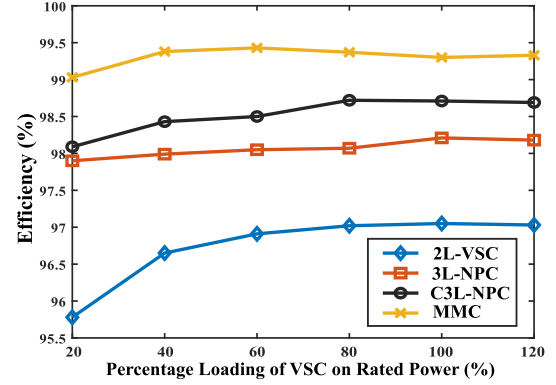


Fig. 9. Efficiency of VSCs over different loading conditions for ± 27 kV with $T_M = 0.5$ years.

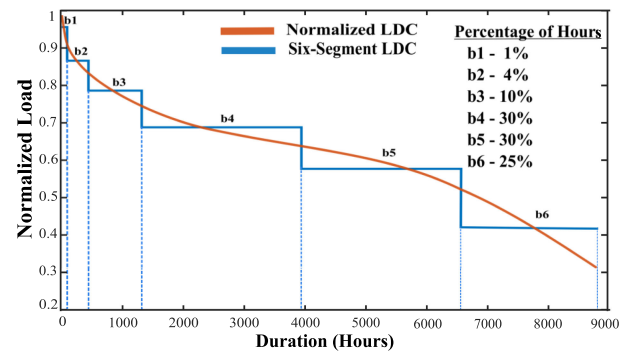


Fig. 10. Normalized and 6-segments load duration curve of the GB in 2019.

TABLE IV
CUMULATIVE ANNUAL ENERGY LOSSES OF EACH VSC (IN MWh)

| | 2L-VSC | 3L-NPC | C3L-NPC | MMC |
|-----------|----------|----------|----------|--------|
| E_{l_x} | 4,400.39 | 2,787.21 | 2,038.35 | 863.78 |

its discretized 6-segment step graph. This discretized 6-segment load duration curve illustrates the average loading of each 6 segments and each segment divided according to the percentage of hours during a year [39], as shown in Fig. 10.

In the operational efficiency analysis of VSCs, instead of using a single average value, this normalized 6-segment load duration curve method provides accurate information to calculate the annual energy produced. The corresponding efficiencies with respect to the loading of the VSCs can be obtained by referring to Figs. 8 and 9. Accordingly, the annual energy losses E_{l_x} (in kWh) of each VSC (where x defines the corresponding VSC) is calculated.

$$E_{l_x} = \left\{ \sum_{b_i=1}^6 (100 - \eta(b_i)) \times t(b_i) \right\} \times P_{VSC} \times 10. \quad (16)$$

where $\eta(b_i)$ and $t(b_i)$ define the efficiency and time (in hours) of the VSC related to the corresponding segment $b_i = 1, 2, \dots, 6$. The term P_{VSC} (in MW) is the rated power of the converter. Table IV shows the cumulative energy losses for each VSC per

TABLE V
 TOTAL COST OF OWNERSHIP OF VSCs (FOR $T_M = 0.5$ IN \$)

| Components | 2L-VSC | 3L-NPC | C3L-NPC | MMC |
|-------------------|---------|---------|---------|-----------|
| IGBT | 328,324 | 328,324 | 555,627 | 681,905 |
| Gate Drive | 31,152 | 31,152 | 52,720 | 64,702 |
| Heat Sink | 37,609 | 37,609 | 63,647 | 78,112 |
| Total Capacitance | 84,590 | 84,590 | 142,801 | 171,379 |
| Power Supply | 21,986 | 21,986 | 37,208 | 45,664 |
| Sensors | 2,038 | 2,038 | 2,038 | 2,038 |
| Control Board | 1,114 | 1,114 | 1,114 | 1,670 |
| NPC diode | N/A | 6,191 | 12,382 | N/A |
| TOTAL | 506,813 | 513,004 | 867,535 | 1,045,470 |

annum for $T_M = 0.5$ years. Due to the lower efficiency of 2L-VSC, the energy losses of each segment is relatively higher than other VSCs.

C. Total Cost of Ownership (TCO)

Depending on the VSC topology, the capital cost, and the operation and maintenance (O&M) costs are varying. The term TCO includes initial investment costs and the O&M cost. However, in this paper, the O&M cost is assumed the same for each VSC considering the same preventive maintenance interval and simplicity.

To perform cost calculations, up-to-date market prices have been obtained through cross-referencing via various manufacturers and distributors [40]. The IGBT unit price is roughly \$2104 for a minimum order quantity of 25 units and the 3L-NPC diodes are \$93/unit. Moreover, the gate drive unit cost of \$189 is accounted per channel and the capacitor energy price is around \$128/kJ [40]. The average exchange rate of 1.277 USD = 1 GBP in 2019 has been considered [41]. Table V summarizes the TCO of each VSC including redundant components.

It should be mentioned that this analysis mainly focuses on the selection of a suitable VSC topology which is the core component in an MVdc converter station. The converter associated plant equipment in a typical VSC substation or MMC SM, such as the cooling plant and interfacing transformers and SM mechanical switch and structural parts, can be further added in the TCO calculation with reliable data (price) input.

The cost of the 3L-NPC is higher than the 2L-VSC due to the additional NPC diodes. Due to more redundant cells in C3L-NPC, (to maintain the same availability) the cost is 69% higher than that of 3L-NPC. The TCO of the MMC is the highest among the four VSCs due to higher part counts.

It is worth mentioning that the actual cost of these VSCs may deviate from the above values due to various non-technical reasons such as confidentiality of cost data and pricing strategies of different manufacturers, time-dependency of component costs due to varying raw material prices and economies of scale. However, project engineers can use their know-how to include more precise component cost factors.

D. Return on Investment (ROI)

In any industrial application, the investment decision is made on how much profit can be gained over its capital investment. This is equally valid in the selection of VSCs which provides

 TABLE VI
 RETURN ON INVESTMENT OF VSCs (± 27 Kv)

| Operational Years | ROI over 2L-VSC | | |
|-------------------|-----------------|---------|------|
| | 3L-NPC | C3L-NPC | MMC |
| $n=1$ | 0.59 | 0.51 | 0.64 |
| $n=5$ | 2.69 | 2.33 | 2.90 |
| $n=10$ | 4.81 | 4.16 | 5.17 |

 TABLE VII
 LEVEL OF REDUNDANCY REQUIRED WITH THE CHANGE OF DC VOLTAGE

| Voltage | 3L-NPC * | | C3L-NPC † | | MMC | |
|-------------|-----------|-------|-----------|-------|-----------|-------|
| | k_{min} | k_R | k_{min} | k_R | k_{min} | k_R |
| ± 10 kV | 4 | 2 | 3 | 3 | 8 | 4 |
| ± 15 kV | 6 | 2 | 4 | 3 | 12 | 4 |
| ± 25 kV | 10 | 3 | 6 | 5 | 20 | 5 |
| ± 35 kV | 14 | 3 | 8 | 7 | 28 | 6 |
| ± 45 kV | 18 | 3 | 10 | 8 | 36 | 6 |
| ± 50 kV | 20 | 3 | 10 | 8 | 40 | 7 |

* required IGBTs per SP † required cells per pole () -redundancy %

a quantitative implication for the financial investment made. The ROI is a quantitative indication of how much profit each dollar invested into that VSC is producing. Thus, a higher ROI is preferred. The topology which shows the highest ROI is selected as the optimal one. To measure the performance of VSCs in terms of ROI, accumulated cost savings relative to 2L-VSC is determined first. The present value of the future cost savings due to energy saving of a VSC can be calculated by

$$S_n = \sum_{i=1}^n \frac{S_i}{(1+k)^i} \quad (17)$$

$$S_i = \sum_{b_i=1}^6 \Delta E_{b_i} \times P_t \quad (18)$$

where S_n is the accumulated cost savings in present value for a period of n years. The term S_i is the cost-saving in year i and k is the annual interest rate. The parameter ΔE_{b_i} (kWh) in (18) defines as the relative energy saving of segment b_i compared to the 2L-VSC. The term P_t (\$/kWh) is the unit of the electricity selling price. For this analysis, $P_t = 0.198$ \$/kWh in the U.K. for the year 2019 has been used [38]. Finally, the ROI is used (19) to measure the VSC investment return (over 2L-VSC), relative to their capital cost.

$$ROI = \frac{S_n}{TCO} \quad (19)$$

Table VI shows the calculated ROI of each VSC with respect to operational years $n = 1, 5$ and 10 assuming a constant annual interest rate of 5% [11]. The topology which shows the highest ROI is selected as the optimal one. Table VI shows that MMC has the highest ROI at ± 27 kV. Even though the initial investment is nearly double of 2L-VSC (as shown in Table V), MMC accounts for the highest energy saving compared to other VSCs. Following the MMC, 3L-NPC shows the second most suitable VSC to be used at ± 27 kV. However, the sensitivity analysis carried out for C3L-NPC shows that, instead of 5 redundant cells, 4 redundant cells are used (at the expense of lower availability) the ROI=0.66 for $n=1$. By doing so, the TCO of C3L-NPC

TABLE VIII
CHARACTERISTICS COMPARISON OF MULTI-LEVEL VSCs AT DIFFERENT DC VOLTAGE LEVELS

| Voltage | Topologies | Efficiency (%) | ROI | Redundancy (%) | TCO (\$) | B ₁₀ life (years) |
|---------|------------|----------------|-------------|----------------|-----------|------------------------------|
| ±10 kV | 3L-NPC | 97.18 | 0.72 | 50 | 224,466 | 0.94 |
| | C3L-NPC | 98.06 | 0.47 | 100 | 422,370 | 1.12 |
| | MMC | 98.81 | 0.49 | 50 | 603,769 | 10.65 |
| ±27 kV | 3L-NPC | 97.18 | 0.59 | 18 | 513,004 | 0.64 |
| | C3L-NPC | 98.26 | 0.51 | 83 | 867,535 | 1.04 |
| | MMC | 99.13 | 0.64 | 22 | 1,045,470 | 5.91 |
| ±50 kV | 3L-NPC | 98.20 | 0.50 | 15 | 884,066 | 0.58 |
| | C3L-NPC | 98.48 | 0.98 | 80 | 1,417,603 | 1.03 |
| | MMC | 99.31 | 1.09 | 18 | 1,699,364 | 5.64 |

can be reduced by 23% which is significant and competitive compared to the MMC.

IV. IMPACT OF RATED DC VOLTAGE AND CURRENT ON TOPOLOGY SELECTION

A. Impact of DC Voltage Level

As discussed in Section II, the selection method of redundant modules for a VSC (to keep the availability above a certain level) is a non-linear process. The required minimum modules and level of redundancy are also different depending on the dc voltage. Thus, the ROI will be different due to variations in TCO and operational efficiencies. In order to observe the impact of dc voltage on topology selection, analyses have been performed from ±10 kV to ±50 kV with a fixed rated current of 500 A. Thus, the power rating varies from 10 MVA to 50 MVA.

Table VII shows the required minimum (k_{\min}) and redundant modules (k_R) for each VSC for some selected MVdc voltage levels with the consideration of the target availability level of 99.99%. It can be noted that with the increase of dc voltage level the redundancy level also increases to keep the same availability. However, as k_{\min} is increased the reliability of the VSC decreases over time due to the stochastic failure nature of PE devices. At low voltage levels, the B₁₀ life is high due to the utilization of a few components.

To observe the voltage ranges in which a particular VSC is the most suitable, variations of ROI against the MVdc voltage are shown in Fig. 11. According to Fig. 11, between ±10 kV and ±24.2 kV (R-1) use of 3L-NPC VSC is more economical than the use of other VSCs. This is because, within these power levels (10–24 MVA), and dc voltage levels 3L-NPC require only a few redundant modules and capital costs do not increase significantly. This makes the increase in capital cost of 3L-NPC does not depend on the redundancy level. Between ±10 kV and ±15 kV the ROI of all the VSCs increase due to the use of the same k_R as of ±10 kV level. However, at ±15 kV the ROI difference between 3L-NPC over C3L-NPC and MMC is relatively higher. This indicates if C3L-NPC or MMC are used at this dc voltage level it will take much longer time to recover the investment. Notably, after ±15 kV the ROI values of C3L-NPC and MMC decrease due to the increase of k_R and relative energy saving is less significant.

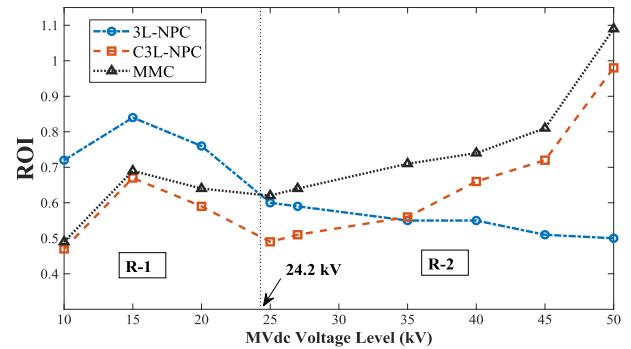


Fig. 11. Variation of ROI with MVdc voltage level (at the rated current of 500 A).

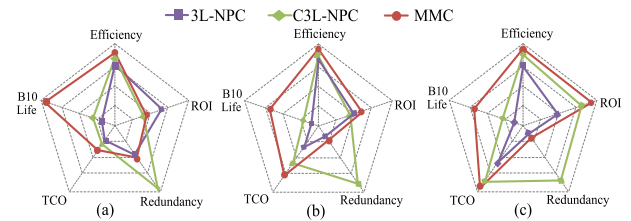


Fig. 12. Comparison of five characteristics of VSCs at different MVdc voltage levels (a) ±10 kV; (b) ±27 kV; and (c) ±50 kV.

Finally, beyond ±24.2 kV (R-2) MMC shows the highest ROI compared to other VSCs owing to the fact that improved efficiencies. This is because at higher MVdc voltage levels more MMC SMs are available to select in the switch selection algorithm. Further, after about ±34 kV C3L-NPC also shows better performance than 3L-NPC, but still inferior to MMC. It should be mentioned that these intersection points may vary depending on the sensitivity of the data.

Table VIII and Fig. 12 summarize the characteristic comparisons of multi-level VSCs based on multiple functional factors discussed above at some selected MVdc voltage levels. The B₁₀ life comparison shows that the MMC has better reliability over the other three VSCs even though the percentage redundancy difference is not much significant compared to 2L-VSC and 3L-NPC. However, with the increase of the dc voltage level, the B₁₀ life decreases irrespective of the VSC due to higher number of components.

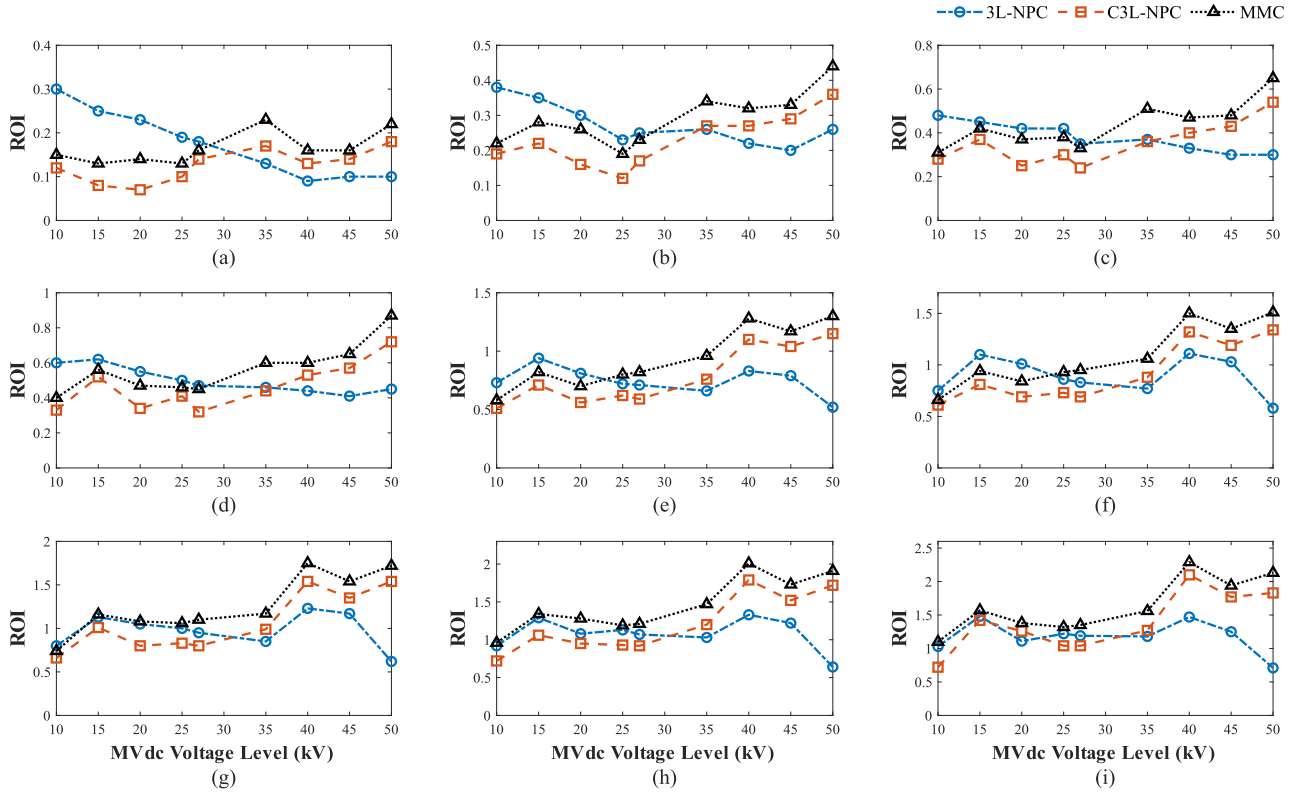


Fig. 13. Variation of ROI with change of rated current at different MVdc voltage levels (a) 100 A; (b) 200 A; (c) 300 A; (d) 400 A; (e) 600 A; (f) 700 A; (g) 800 A; (h) 900 A; and (i) 1000 A.

B. Impact of Rated Current

The selection of VSC topologies at different MVdc voltage levels for a fixed rated capacity has been discussed in the above section. Further analysis in identifying a suitable VSC topology with the variation of its rated current has been carried out in this section. In this study, the 3L-NPC, C3L-NPC and MMC are selected as the candidates. As shown in Fig. 13, the converter rated current has been changed from 100 A to 1000 A and the same MVdc voltage class (from ± 10 kV to ± 50 kV) has been considered. This corresponds to a broader spectrum of analysis of converter power ratings which ranges from 2 MVA to 100 MVA.

From Fig. 13, it can be observed that irrespective of the MVdc voltage level, the ROI increases with the increase of converter rated current. This is due to the fact that, at higher current levels converter exports more energy than at lower current levels. This results in higher accumulated cost savings for the period considers. The general trend for 3L-NPC is that the ROI decreases with the increase of the voltage level irrespective of the converter rating. On the contrary, the ROI of MMC and C3L-NPC shows an increasing trend. For the current range considered in this analysis, between ± 30 kV and ± 35 kV, C3L-NPC crosses over 3L-NPC. However, as mentioned in Section IV-A, its ROI is still lower compared to MMC.

Fig. 14 summarizes different MVdc crossover voltage levels in which a candidate VSC topology is suitable under a specific rated current. At current levels below 400 A and voltage level

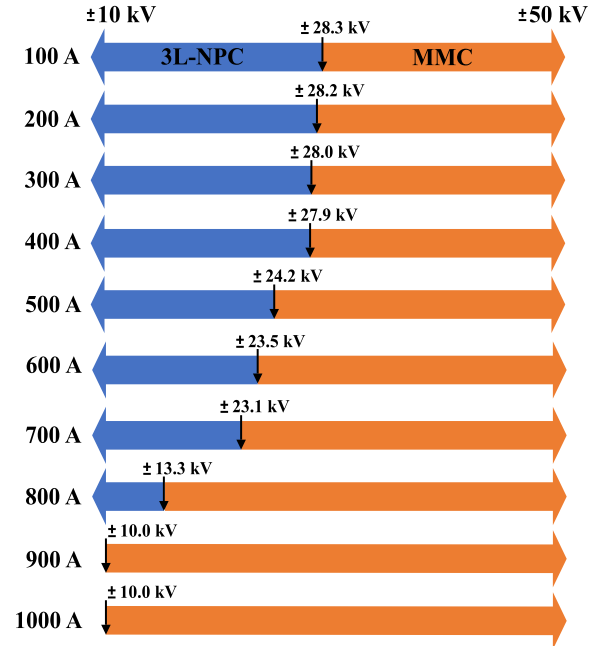


Fig. 14. Variation of voltage crossover points with the change of rated currents.

below ± 28 kV, the use of 3L-NPC is more beneficial. Beyond 900 A, the use of MMC is more economical for the whole MVdc voltage spectrum discussed here.

V. CONCLUSION

To obtain overall techno-economic benefits from MVdc technology, a suitable converter topology is required. This paper presents a systematic criterion to select multi-level VSC for MVdc applications taking the reliability, redundancy, efficiency and economic feasibility factors such as TCO and ROI into account. To obtain the optimum redundancy level for VSCs, a preventive maintenance based approach is used with a pre-defined availability level. A method based on normalized six-segment load duration curve is introduced to assess the operational efficiencies and thereby to evaluate feasibilities of VSCs at different MVdc voltage levels.

The analysis performed here reveals that below 400 A and ± 28 kV MVdc voltage level, use of 3L-NPC VSC is much more cost-effective since it provides higher investment return (due to lower capital cost and redundancy). Between 500 A and 700 A and above ± 23 kV, the use of MMC is more economical. However, the study suggests that with the increase of MVdc voltage level and higher current levels, the use of MMC is financially beneficial and is also more reliable than other converter topologies. Additionally, beyond about ± 35 kV, C3L-NPC can also be considered as an alternative option for MMC.

REFERENCES

- [1] L. Zhang *et al.*, "Converting AC distribution lines to DC to increase transfer capacities and DG penetration," *IEEE Trans. Smart Grid*, vol. 10, no. 2, pp. 1477–1487, Mar. 2019.
- [2] C. Dincan *et al.*, "A high-power, medium-voltage, series-resonant converter for DC wind turbines," *IEEE Trans. Power Electron.*, vol. 33, no. 9, pp. 7455–7465, Sep. 2018.
- [3] G. Li *et al.*, "Comparisons of MVAC and MVDC systems in dynamic operation, fault protection and post-fault restoration," in *Proc. 45th Annu. Conf. IEEE Indus. Electron. Soc.*, vol. 1, 2019, pp. 5657–5662.
- [4] X. Yang *et al.*, "An improved droop control strategy for VSC-Based MVDC traction power supply system," *IEEE Trans. Ind. Appl.*, vol. 54, no. 5, pp. 5173–5186, Sep./Oct. 2018.
- [5] R. M. Cuzner and V. Singh, "Future shipboard MVdc system protection requirements and solid-state protective device topological tradeoffs," *IEEE Trans. Emerg. Sel. Top. Power Electron.*, vol. 5, no. 1, pp. 244–259, Mar. 2017.
- [6] C. Yuan, M. A. Haj-ahmed, and M. S. Illindala, "Protection strategies for medium-voltage direct-current microgrid at a remote area mine site," *IEEE Trans. Ind. Appl.*, vol. 51, no. 4, pp. 2846–2853, Jul./Aug. 2015.
- [7] H. Krishnamoorthy *et al.*, "Isolated AC-DC converter using medium frequency transformer for offshore wind turbine DC collection grid," *IEEE Trans. Ind. Electron.*, vol. 64, no. 11, pp. 8939–8947, Nov. 2017.
- [8] G. Abeynayake, G. Li, J. Liang, and N. A. Cutululis, "A review on MVdc collection systems for high-power offshore wind farms," in *Proc. 14th Conf. Indus. Infor. Syst.*, 2019, pp. 407–412.
- [9] R. M. Burkart and J. W. Kolar, "Comparative life cycle cost analysis of Si and SiC PV converter systems based on advanced η - ρ - σ multiobjective optimization techniques," *IEEE Trans. Power Electron.*, vol. 32, no. 6, pp. 4344–4358, Jun. 2017.
- [10] R. Teichmann and S. Bernet, "A comparison of three-level converters versus two-level converters for low-voltage drives, traction, and utility applications," *IEEE Trans. Ind. Appl.*, vol. 41, no. 3, pp. 855–865, May/Jun. 2005.
- [11] E. Kantar and A. M. Hava, "Optimal design of grid-connected voltage-source converters considering cost and operating factors," *IEEE Trans. Ind. Electron.*, vol. 63, no. 9, pp. 5336–5347, Sep. 2016.
- [12] T. B. Sоеiro and J. W. Kolar, "Analysis of high-efficiency three-phase two- and three-level unidirectional hybrid rectifiers," *IEEE Trans. Ind. Electron.*, vol. 60, no. 9, pp. 3589–3601, Sep. 2013.
- [13] "IEEE recommended practice and requirements for harmonic control in electric power systems," IEEE Std 519-2014 (*Revision of IEEE Std 519-1992*), pp. 1–29, 2014.
- [14] G. Li, C. Li, and D. VanHertem, "HVDC technology overview," in *HVDC Grids for Offshore and Supergrid of the Future*, D. Van Hertem, O. Gomis-Bellmunt, and J. Liang, Eds. Hoboken, NJ, USA: Wiley IEEE Press, 2016, ch. 3, pp. 45–78.
- [15] G. Li *et al.*, "Feasibility and reliability analysis of LCC DC grids and LCC/VSC hybrid DC grids," *IEEE Access*, vol. 7, pp. 22 445–22 456, 2019.
- [16] M. Mirjafari, S. Harb, and R. S. Balog, "Multiobjective optimization and topology selection for a module-integrated inverter," *IEEE Trans. Power Electron.*, vol. 30, no. 8, pp. 4219–4231, Aug. 2015.
- [17] J. Guo, X. Wang, J. Liang, H. Pang, and J. Gonçaves, "Reliability modeling and evaluation of MMCs under different redundancy schemes," *IEEE Trans. Power Del.*, vol. 33, no. 5, pp. 2087–2096, Oct. 2018.
- [18] G. Abeynayake, J. Yu, A. Moon, and J. Liang, "Analysis and control of MVDC demonstration project in the U.K.: ANGLE-DC," *Power Supply*, vol. 37, no. 10, pp. 44–50, 2020.
- [19] L. Qu *et al.*, "Planning and analysis of the demonstration project of the MVDC distribution network in zhuhai," *Front. Energy*, vol. 13, no. 1, pp. 120–130, 2019.
- [20] F. Mura and R. W. De Doncker, "Design aspects of a medium-voltage direct current (MVDC) grid for a university campus," in *Proc. 8th Int. Conf. Power Electron.-ECCE Asia*, 2011, pp. 2359–2366.
- [21] Y. Gao *et al.*, "Study on fault current characteristics and current limiting method of plug-in devices in VSC-DC distribution system," *Energies*, vol. 12, no. 3159, 2019.
- [22] H. A. B. Siddique *et al.*, "Comparison of modular multilevel and neutral-point-clamped converters for medium-voltage grid-connected applications," in *Proc. IEEE Int. Conf. Renewable Energy Res. Appl.*, 2016, pp. 297–304.
- [23] J. Xu, P. Zhao, and C. Zhao, "Reliability analysis and redundancy configuration of MMC with hybrid submodule topologies," *IEEE Trans. Power Electron.*, vol. 31, no. 4, pp. 2720–2729, Apr. 2016.
- [24] G. Konstantinou, J. Pou, S. Ceballos, and V. G. Agelidis, "Active redundant submodule configuration in modular multilevel converters," *IEEE Trans. Power Del.*, vol. 28, no. 4, pp. 2333–2341, Oct. 2013.
- [25] P. Tu, S. Yang, and P. Wang, "Reliability- and cost-based redundancy design for modular multilevel converter," *IEEE Trans. Power Electron.*, vol. 66, no. 3, pp. 2333–2342, Mar. 2019.
- [26] J. Guo *et al.*, "Reliability analysis of MMCs considering submodule designs with individual or series-operated IGBTs," *IEEE Trans. Power Del.*, vol. 32, no. 2, pp. 666–677, Apr. 2017.
- [27] U. Choi, F. Blaabjerg, and K. Lee, "Study and handling methods of power IGBT module failures in power electronic converter systems," *IEEE Trans. Power Electron.*, vol. 30, no. 5, pp. 2517–2533, May 2015.
- [28] J. Yu *et al.*, "Initial designs for angle-dc project: Challenges converting existing ac cable and overhead line to dc operation," *CIGRE - Open Access Proc. J.*, vol. 2017, no. 1, pp. 2374–2378, 2017.
- [29] T. Joseph *et al.*, "Dynamic control of MVDC link embedded in distribution network:-case study on ANGLE-DC," in *Proc. IEEE Conf. Energy Int. Energy Syst. Integration*, 2017, pp. 1–6.
- [30] J. Peralta, H. Saad, S. Denneriere, J. Mahseredjian, and S. Nguеfeu, "Detailed and averaged models for a 401-Level MMC-HVDC system," *IEEE Trans. Power Del.*, vol. 27, no. 3, pp. 1501–1508, Jul. 2012.
- [31] F. Richardeau and T. T. L. Pham, "Reliability calculation of multilevel converters: Theory and applications," *IEEE Trans. Ind. Electron.*, vol. 60, no. 10, pp. 4225–4233, Oct. 2013.
- [32] J. Wylie, "Reliability analysis of modular multi-level converters for high and medium voltage applications," Ph.D. dissertation, Dept. Elect. Electron. Eng., Imperial College London, 2019.
- [33] T. Joseph *et al.*, "Asset management strategies for power electronic converters in transmission networks: Application to HVDC and FACTS devices," *IEEE Access*, vol. 6, pp. 21 084–21 102, 2018.
- [34] D. Rock, "Guidance on the Offshore Transmission Owner Licence for Tender Round 5 (TR5)," Ofgem, pp. 1–39, 2017.
- [35] N. S. Dhaliwal *et al.*, "CIGRE WG B4.04: Converter transformer failure survey results from 2003 to 2012," CIGRE TB-617, Tech. Rep. 280, 2015.
- [36] Power semiconductors Semiconductors Product Catalog 2020. [Online]. Available: <https://new.abb.com/semiconductors>
- [37] *PLECS- the Simulation Platform for Power Electronic Systems, 4th ed.*, Plexim, Plexim, GmbH, Zurich, Switzerland, 2019.

- [38] “Summer outlook 2019,” *Nat. Grid*, U.K., Tech. Rep. 19, 2019. [Online]. Available: <https://www.nationalgrid.com/document/111936>
- [39] W. Jaglom *et al.*, “Assessment of projected temperature impacts from climate change on the U.S. electric power sector using the integrated planning model,” *Energy Policy*, vol. 73, pp. 524–539, 2014.
- [40] Electronic Components. Mouser Electronics, U.K. [Online]. Available: <https://www.mouser.co.uk>
- [41] Bank of England Database. Exchange Rate 2019 - GBP to USD. [Online]. Available: <https://www.bankofengland.co.uk/boeapps/database>



Gayan Abeynayake (Graduate Student Member, IEEE) received the B.Sc.Eng. degree (Hons.) in electrical and electronic engineering and the M.Sc.Eng. degree in power, energy systems and high voltage from the University of Peradeniya, Sri Lanka, in 2011 and 2016, respectively. Since April 2018, he has been working toward the Ph.D. degree in electrical engineering with Cardiff University, Cardiff, U.K. From 2012 to 2018, he was a Transmission Planning Engineer with Ceylon Electricity Board, Colombo, Sri Lanka. He is currently a Chartered Electrical

Engineer with the Institution of Engineers, Sri Lanka. He is also a Marie Curie Early Stage Research Fellow with Cardiff University, working on the InnoDC project. In 2019, he was a Visiting Researcher with the Technical University of Denmark (DTU), Risø, Denmark. Between February to June 2020, he was a Research Associate with the National Grid Project, U.K., on “demand side flexibility from Industrial and Commercial Users. His main research interests include power electronics applications in MVdc systems, power systems, and power electronics reliability, grid integration of renewable energy, and power system planning. He was the recipient of the Prof. E.O.E Pereira Gold Medal for the Most Outstanding Engineering Graduate at the General Convocation 2012 and received the 1st prize of the IEEE PES UKRI presentation competition, Cardiff, in 2018. He is the Secretary of the IEEE PELS Society U.K.&I chapter for the term 2020–2021.



Gen Li (Member, IEEE) received the B.Eng. degree in electrical engineering and automation from Northeast Electric Power University, Jilin City, China, in 2011, the M.Sc. degree in power engineering from Nanyang Technological University, Singapore, in 2013, and the Ph.D. degree in electrical engineering from Cardiff University, Cardiff, U.K., in 2018. From 2013 to 2016, he was a Marie Curie Early Stage Research Fellow funded by the European Union’s MEDOW Project. He has been a Visiting Researcher with China Electric Power Research Institute and Global Energy Interconnection Research Institute, Beijing, China, Elia, Brussels, Belgium, and Toshiba International (Europe), London, U.K. Since 2017, he has been a Research Associate with the School of Engineering, Cardiff University. His research interests include control and protection of HVDC and MVDC technologies, power electronics, reliability modeling, and evaluation of power electronics systems. Dr. Li is a Chartered Engineer in the U.K. He is an Associate Editor for the *CSEE Journal of Power and Energy Systems*. He is an Editorial Board Member of *CIGRE ELECTRA*. He was the recipient of the First CIGRE Thesis Award in 2018 for his Ph.D. thesis.



Tibin Joseph (Member, IEEE) received the B.Tech. and M.Tech. degrees in electrical engineering from Mahatma Gandhi University, Kerala, India, in 2008 and 2011, respectively, and the Ph.D. degree in electrical and electronic engineering from Cardiff University, Wales, U.K., in 2018. From 2012 to 2013, he was a Lecturer with the Saintgits College of Engineering, Kerala, India. Between 2013 and 2016, he was a Marie Curie Early-Stage Researcher with Cardiff University. He has been a Visiting Researcher with China Electric Power Research Institute, Beijing, China, and

with National Grid, Warwick, U.K. From 2016 to 2020, he was a Research Associate with Cardiff University, working on the ANGLE-DC Project. He is currently a Power Systems Engineer with Energy Systems Catapult, U.K. His main research interests include power electronics application in power systems, grid integration of renewable energy, and power system control and stability.



Jun Liang (Senior Member, IEEE) received the B.Sc. degree in electric power system and its automation from the Huazhong University of Science and Technology, Wuhan, China, in 1992, and the M.Sc. and Ph.D. degrees in electric power system and its automation from China Electric Power Research Institute (CEPRI), Beijing, China, in 1995 and 1998, respectively. From 1998 to 2001, he was a Senior Engineer with CEPRI, from 2001 to 2005, he was a Research Associate with Imperial College London, London, U.K., and from 2005 to 2007, he was a Senior

Lecturer with the University of Glamorgan, Wales, U.K. He is a Professor in power electronics with the School of Engineering, Cardiff University, Cardiff, U.K. He is the Coordinator and Scientist-in-Charge of two European Commission Marie-Curie Action ITN/ETN projects, MEDOW (€ 3.9 M) and InnoDC (€ 3.9 M). His research interests include HVDC, MVDC, FACTS, power system stability control, power electronics, and renewable power generation. Prof. Liang is a Fellow of the Institution of Engineering and Technology, the Chair of the IEEE U.K. and Ireland Power Electronics Chapter, an Editorial Board Member of the *CSEE JPES*, and the Editor of the *IEEE TRANSACTIONS ON SUSTAINABLE ENERGY*.



Wenlong Ming (Member, IEEE) received the B.Eng. and M.Eng. degrees in automation from Shandong University, Jinan, China, in 2007 and 2010, respectively, and the Ph.D. degree in automatic control and systems engineering from the University of Sheffield, Sheffield, U.K., in 2015. Since August 2020, he has been a Senior Lecturer of power electronics with Cardiff University, Cardiff, U.K., and since April 2020, he has been a Senior Research Fellow funded by Compound Semiconductor Applications (CSA) Catapult, U.K., for five years. In 2012, he was with

Center for Power Electronics Systems (CPES), Virginia Tech, Blacksburg, VA, USA, as an Academic Visiting Scholar. He has coauthored more than 50 papers published in leading journals or refereed IEEE conferences. His research interests include medium voltage dc systems for electricity distribution networks, and characterization, modeling, and applications of wide-bandgap compound semiconductors. He was the recipient of the prestigious IET Control & Automation Doctoral Dissertation Prize in 2017.